AIAA JOURNAL
Vol. 49, No. 11, November 2011

# Simulation of Cryogenics Cavitation

Sean Kelly* and Corin Segal†
*University of Florida, Gainesville, Florida 32611*
and
John Peugeot‡
*NASA Marshall Space Flight Center, Huntsville, Alabama 35811*

DOI: 10.2514/1.J051033

**Cavitation in cryogenic fluids was simulated on a NACA 0015 hydrofoil in a closed-loop facility filled with a perfluorinated ketone that exhibits a strong thermodynamic effect at ambient conditions. Static pressures were measured at seven locations along the hydrofoil chord and along the wall of the test section. Speeds up to 7.5 m/s and temperatures up to 40°C showed the formation and collapse of vapor bubbles in regimes ranging from incipient cavitation to supercavitation. Effects of velocity, cavitation number, and temperature were studied. For the two lower inlet temperature cases, cavitation was observed before the local static pressure dropped to the saturation pressure corresponding to the inlet temperature. Pressure and frequency analysis of this phenomenon is described below.**



## Nomenclature

| | | |
|---|---|---|
| $c$ | = | chord length, m |
| $C_p$ | = | pressure coefficient; $(P - P_\infty)/\frac{1}{2}\rho_\infty U_\infty]$ |
| $c_{p,l}$ | = | specific heat of liquid phase, kJ/kg · K |
| $f$ | = | frequency, Hz |
| $k$ | = | thermal conductivity, W/m · K |
| $P$ | = | static pressure, Pa |
| $P_o$ | = | stagnation pressure, Pa |
| $Pr$ | = | Prandtl number; $C_{p,l}\mu/k$ |
| $Re$ | = | Reynolds number; $U_\infty c/v$ |
| $St_c$ | = | Strouhal number, based on chord length; $fc/U_\infty$ |
| $U$ | = | velocity, m/s |
| $\alpha$ | = | angle of attack, deg |
| $\Delta H_{\text{vap}}$ | = | heat of vaporization, kJ/kg |
| $\Delta T$ | = | local temperature depression due to thermodynamic effect |
| $\Delta T^*$ | = | thermodynamic effect, K |
| $\mu$ | = | dynamic viscosity, kg/m · s |
| $v$ | = | kinematic viscosity, $m^2/s$ |
| $\rho$ | = | density, $kg/m^3$ |
| $\sigma$ | = | cavitation number |

*Subscripts*

| | | |
|---|---|---|
| $l$ | = | liquid phase |
| $v$ | = | vapor phase |
| $\infty$ | = | freestream condition |

## I. Introduction

CRYOGENIC fuels used in modern rocket engines are often pumped in the regime close to cavitation, a condition that can lead to damage, performance degradation, and even system failure. Turbopumps moving cryogenics encounter different complications than those experienced during inducer performance in more common liquids. Cavitation is often studied using water, given the practical difficulties of cryogenics testing, yet cavity formation in cryogenic fluids is subject to vaporization and bubble formation in a different way than in other, nonthermosensitive fluids, such as water. There exists no rigorous correlation of pump suction performance and cavitation instabilities in cryogenic liquids and in water.

A main nondimensional parameter describing the process is the cavitation number, defined as

$$\sigma = \frac{P_\infty - P_v}{1/2\rho_\infty U_\infty^2} \tag{1}$$

Generally, cavitation can be described as the formation of vapor bubbles due to the local static pressure dropping to the saturation vapor pressure, which corresponds to the cavitation number in the flow being equal to $(-Cp)$. Since the vapor pressure is a function of temperature, thermal energy is absorbed when the fluid vaporizes. This effect is strong in fluids sensitive to this temperature drop, such as cryogenics, and leads to a cavitation number not equal to $(-Cp)$.

For water, this temperature change is insignificant, hence leading to inaccurate simulation of cavitation in turbopumps; for liquid propellants and other cryogenics, this temperature change must be considered.

This effect can be estimated based on a scaling suggested by Franc et al. [1]:

$$\Delta T = \Delta T^* \cdot Pr^{0.7} \cdot Re^{0.2} \tag{2}$$

where

$$\Delta T^* = \frac{\Delta H_{\text{vap}}}{C_{p,l}} \frac{\rho_v}{\rho_l} \tag{3}$$

At ambient conditions, water exhibits a $\Delta T^*$ approximately 10 times smaller than the working fluid used here, perfluorinated ketone 2-trifluoromethyl-1,1,1,2,4,4,5,5,5-nonafluoro-3-pentanone, or $CF_3CF_2C(O)CF(CF_3)_2$, hereafter known as fluoroketone, and two orders of magnitude smaller than rocket propellant liquid hydrogen at operating conditions. This low $\Delta T^*$ is due to the large density ratio $\rho_l/\rho_v$ in water and is hard to match values associated with cryogenic fluids due to the experimental difficulties in reaching the critical point of water.

Fluids that exhibit a low $\Delta T^*$ show discreet vapor and liquid phases, whereas cryogenics and other fluids with a high $\Delta T^*$ tend

Presented as Paper 2011-0808 at the 49th AIAA Aerospace Sciences Meeting including the New Horizons Forum and Aerospace Exposition , Orlando, FL, 4–7 January 2011; received 26 October 2010; revision received 16 May 2011; accepted for publication 6 June 2011. 

*Graduate Research Assistant, Mechanical and Aerospace Engineering, MAE-A 231, Post Office Box 116250. Member AIAA.

†Professor, Mechanical and Aerospace Engineering, MAE-A 231, Post Office Box 116250. Associate Fellow AIAA.

‡Aerospace Engineer.

**Table 1 Key cavitation properties for various fluids**

| Fluid | $T$, K | $P_v$, kPa | $\Delta T^*$, K | $\rho_l/\rho_v$ |
|---|---|---|---|---|
| Water | 298 | 3.2 | 0.014 | 43,229 |
| | 323 | 12.4 | 0.05 | 11,889 |
| | 343 | 31.2 | 0.11 | 4,927 |
| Fluoroketone | 298 | 40.4 | 0.26 | 288 |
| | 323 | 104 | 0.67 | 118 |
| | 343 | 197 | 1.22 | 60 |
| Hydrogen | 22 | 159 | 1.189 | 34 |

to contain a frothy two-phase mixture [2]. Because of the compressibility of these mixtures, their low speeds of sound, often only a few meters per second, can produce effects such as choking and shock waves [3]. Fluoroketone has a low kinematic viscosity, allowing high-$Re$ testing at low speeds.

Fluoroketone alleviates cryogenic testing difficulties and facilitates the study of cavitation effects in thermosensitive fluids at ambient conditions. When heated to 70°C, fluoroketone has a $\Delta T^*$ identical to liquid hydrogen at its working conditions. As an example, values of $\Delta T^*$ for several fluids are given in Table 1. The density ratio of water is two to three orders of magnitude larger than that of fluoroketone and hydrogen. This, in addition to the higher vapor pressures of these thermosensitive fluids, shows the greater propensity toward cavitation due to the effect of $\Delta T^*$ and the cavitation number $\sigma$. Cavitation in fluoroketone occurs at higher cavitation numbers than in water, roughly twice the value as reported by Gustavsson et al. [4]. Finally, the fluid is less reactive, and hence less likely to suffer inaccuracies in the results due to impurities.

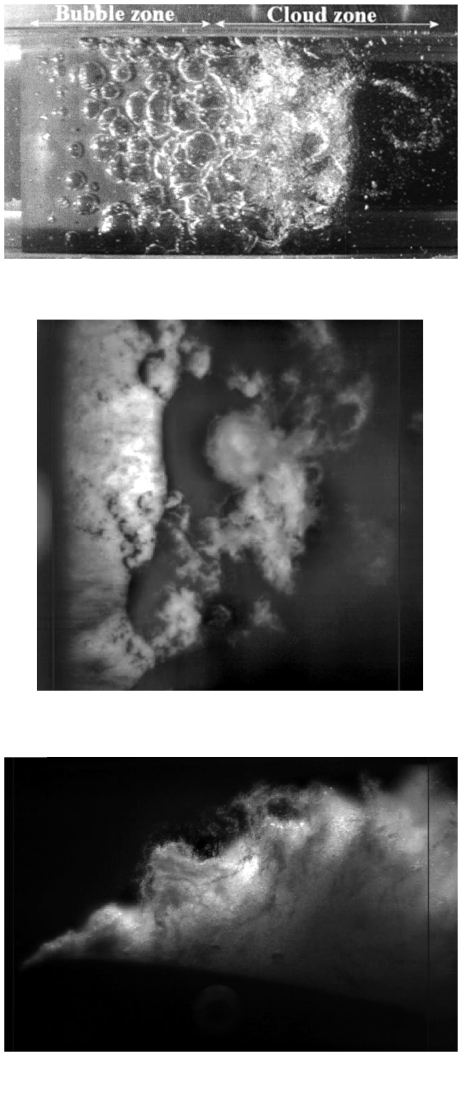


**Fig. 1 Examples of different cavitation regimes: a) top view of cavitation in water; supercavitation in fluoroketone from b) top and c) side.**

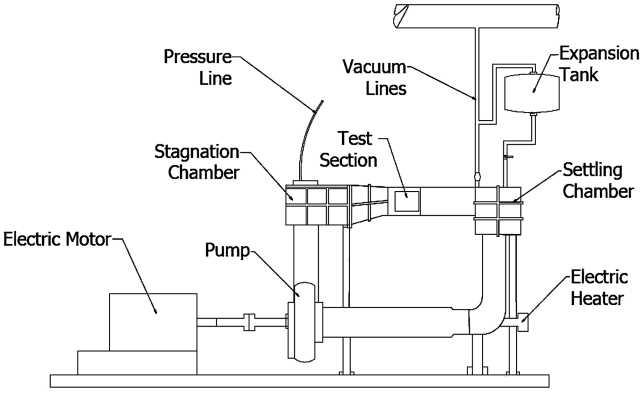


**Fig. 2 Sketch of tunnel facility used in experiments.**

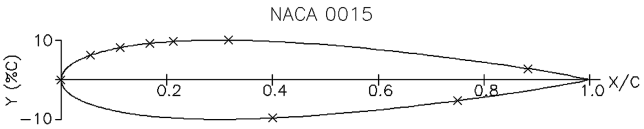


**Fig. 3 Schematic of hydrofoil with pressure taps indicated by Xs.**

Cavitation has historically [5] been relegated to three regimes based on the severity of the vapor formation. The first regime occurs upon the transformation from cavitation-free flow to the point where the first vapor bubbles can be detected, called incipient cavitation. Next, when these bubbles coalesce to form a cavity, it is identified appropriately as cloud cavitation, which is typically the most unsteady regime, oscillating roughly between 50 and 75% of the chord length of the hydrofoil. Supercavitation occurs when the cavity grows in size to extend beyond the hydrofoil or control surface.

**Table 2 Experimental conditions**

| Case | Angle of attack, deg | Temperature, C | $U_\infty$. m/s | $\sigma$ | $P_\infty$, psi |
|---|---|---|---|---|---|
| 1 | 7.5 | 25 | 6 | 1.5 | 12.1 |
| 2 | 7.5 | 25 | 6 | 0.7 | 9.1 |
| 3 | 7.5 | 25 | 7.5 | 0.7 | 11 |
| 4 | 7.5 | 30 | 7.5 | 0.7 | 12.2 |
| 5 | 7.5 | 40 | 7.5 | 0.7 | 15.6 |

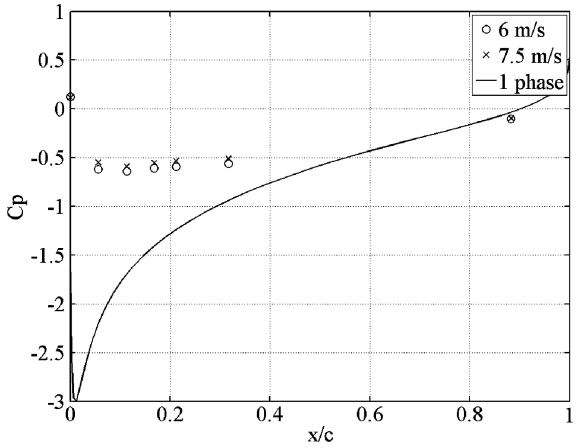


**Fig. 4 Pressure coefficient over a cavitating NACA 0015 hydrofoil in fluoroketone with varying tunnel speed at fixed angle of attack of 7.5 deg, temperature 25°C, and cavitation number $\sigma = 0.7$.**

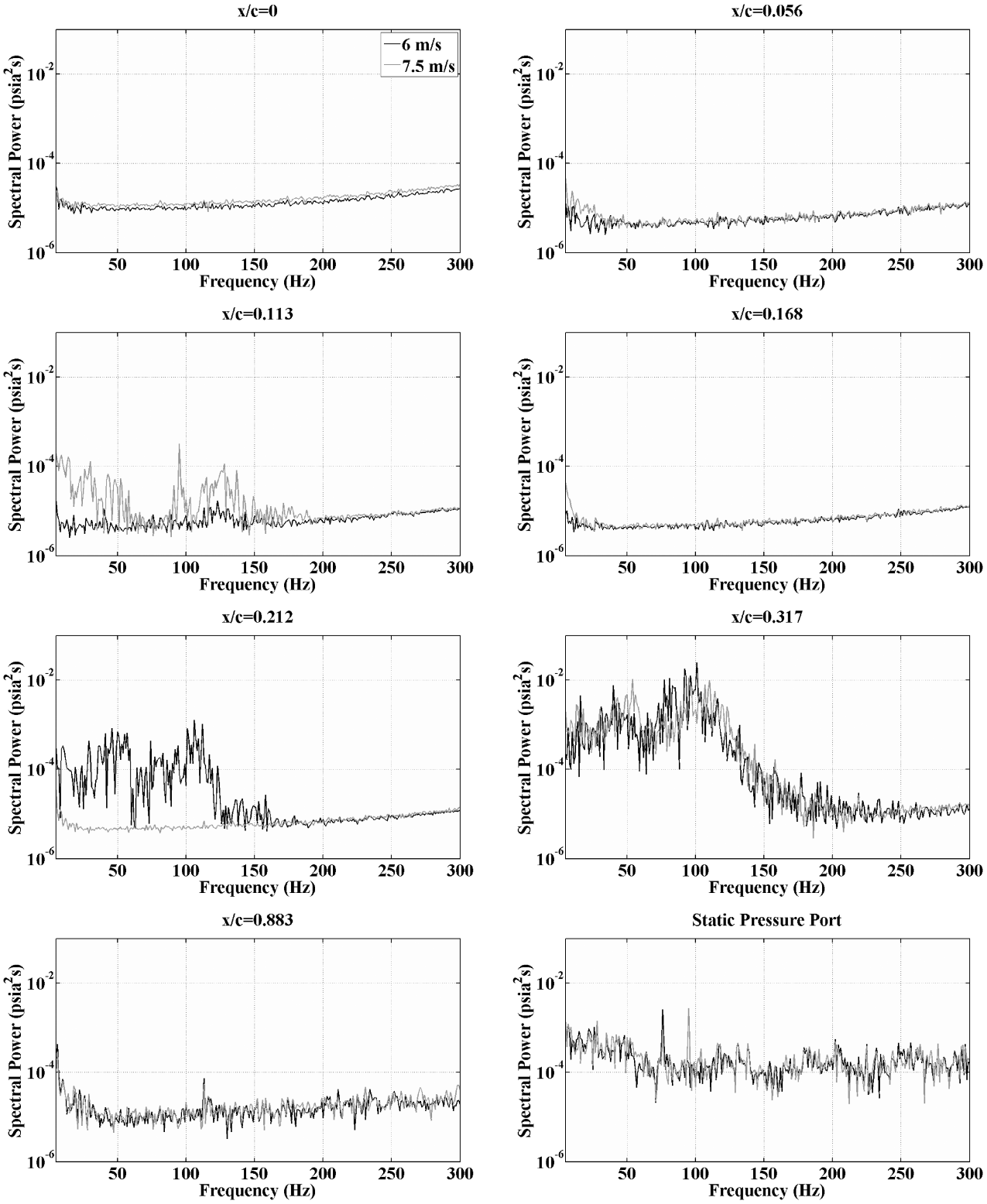


**Fig. 5 Power spectra at various positions along the chord of a cavitating NACA 0015 hydrofoil in fluoroketone with varying tunnel speed at fixed angle of attack of 7.5 deg, temperature 25°C, and cavitation number $\sigma = 0.7$.**

Figure 1 shows several instances of cavitation, in both water and fluoroketone. Figure 1a is a view from above a NACA 0015 hydrofoil at $\sigma = 1.25$ in water, with flow from left to right. Compared with Fig. 1b, another top view of cloud cavitation in fluoroketone at $\sigma = 0.7$, the differences in bubble size are obvious, as well as the difference in the development of the cloud along the hydrofoil surface. Figure 1c shows the height of the vapor cavity in supercavitation of fluoroketone at $\sigma = 0.7$ from a side view, with flow from left to right. In Figs. 1a and 1b, the vertical lines indicate leading and trailing edges of the same model hydrofoil as Fig. 1a.

The dominant frequency of the oscillations in a cavitating flow is typically normalized by a Strouhal number based on chord length, as seen in Eq. (4):

$$St_c = \frac{fc}{U_\infty} \tag{4}$$

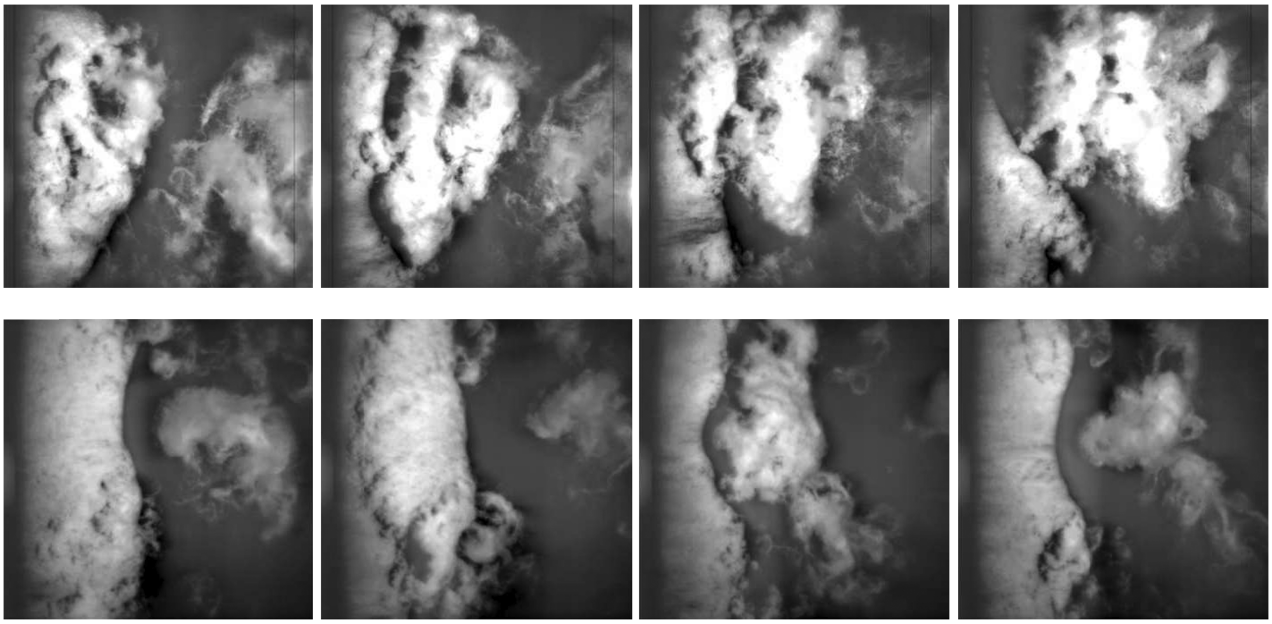

**Fig. 6 Top view of the hydrofoil in case 2 (top) and case 3 (bottom).**



## II. Experimental Setup

### A. Facility

A closed-loop tunnel with a $100 \times 100$ mm cross section was constructed for these experiments and filled with fluoroketone. The facility is designed to operate at pressures up to 0.5 MPa. The tunnel shown schematically in Fig. 2 is driven by a 25 hp motor that allows the speed of the pump to be controllably varied. The system is capable of delivering 0.11 $m^3/s$, which can sustain 10 m/s in the test section at ambient conditions. A stagnation chamber upstream of the test section eliminates possible bubbles formed in the pump and is fitted with mesh screens that filter and help to straighten the flow. Downstream of the test section, there is a settling chamber designed to inhibit large-scale low-frequency oscillations in the flow due to mass redistribution. An expansion tank accounts for volume changes to maintain the required pressure during the experiments. A vacuum system allows static pressure to be lowered to achieve lower cavitation numbers in the flow.

The tunnel is equipped with Omega pressure transducers in the stagnation chamber, settling chamber, and along the bottom wall of the test section upstream of the hydrofoil. The uncertainty of these transducers is 1.2% full scale, or 2.5 kPa. The pump outlet is equipped with a Prandtl probe to monitor flow speed. All sensor outputs were recorded at 1 kHz during the tests. The tunnel is fitted with a submersion heater and a degassing system to remove dissolved oxygen.

The test section has optical access via glass windows on the top and front sides. The hydrofoil can be positioned at an angle of attack of $\pm 10$ deg. Images were taken at 500 frames per second by a Cooke Corporation charge-coupled device camera. Exposure time is 10 $\mu$s.

### B. Hydrofoil

A NACA 0015 hydrofoil with a chord length of $c = 50.8$ mm and span of 100 mm was used in the study. Pressure taps are located at $x/c = 0.0$, 0.056, 0.112, 0.168, 0.212, 0.317, and 0.883 along the suction side and $x/c = 0.40$ and 0.75 along the pressure side, as shown in Fig. 3. To reduce response time, each tap is fitted to a pressure transducer using tubing filled with the working fluid. Analysis indicated that frequencies in the range of interest (i.e., below 500 Hz) are not damped in these tubes.

## III. Test Conditions

A table of experimental conditions is shown in Table 2. The tests were designed to isolate the effects of several experimental parameters. Comparison of tests 1 and 2 shows the effect of cavitation number while holding constant the temperature and velocity. Similarly, comparing results from tests 2 and 3 indicates the effect of freestream velocity, while cases 3, 4, and 5 compare temperature variations.

## IV. Results and Discussion

$Cp$ curves, power spectral density (PSD) plots, and sets of image series for the flow parametrics of temperature, cavitation, and velocity are shown in Figs. 4–12. For each case, plotted data are organized by position along the hydrofoil, with the addition of the static pressure port PSD to show the freestream flow conditions, and images are shown adjacent to visually highlight the differences in each flow.

The $Cp$ curves show differences in the flow between different cases very clearly. The shape of the $Cp$ curve changes most dramatically with the variation of cavitation number, as the transition between incipient cavitation, cloud cavitation, and supercavitation proceed, respectively, with reduced cavitation number. The $Cp$ for all low-temperature cases at 25°C (Figs. 4 and 7) was more than $(-\sigma)$, which indicates that fully developed supercavitation exists for pressures above the freestream vapor pressure without the effects of heat transfer via $\Delta T^*$.

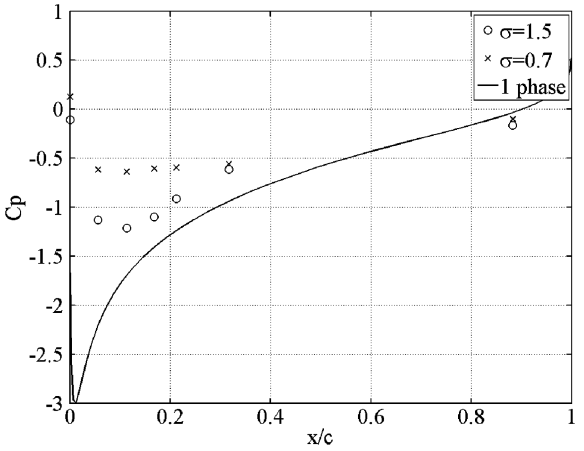


**Fig. 7 Pressure coefficient over a cavitating NACA 0015 hydrofoil in fluoroketone with varying cavitation number at fixed angle of attack of 7.5 deg, temperature 25°C, and freestream velocity 6 m/s.**

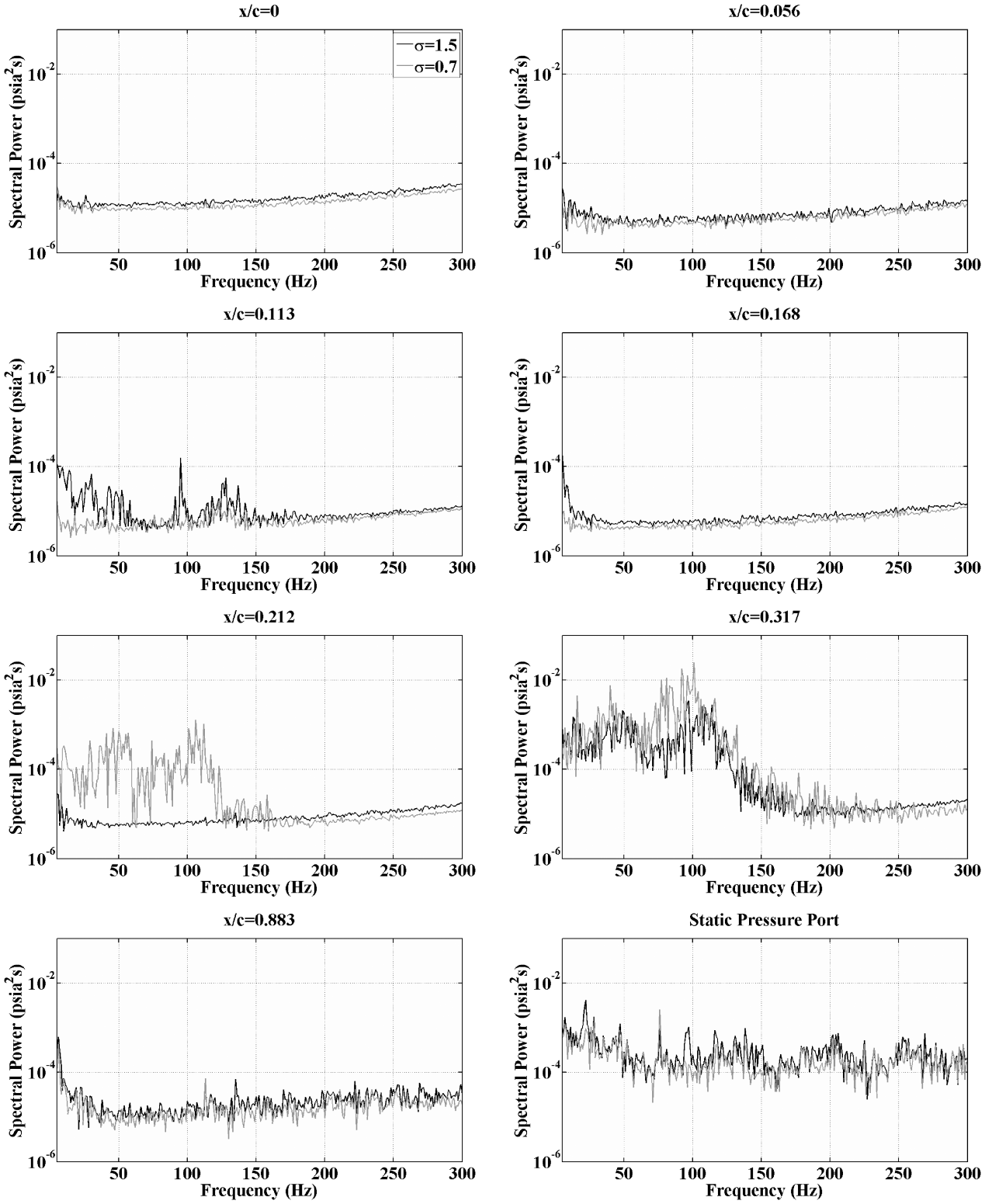


**Fig. 8 Power spectra of static pressure and at various positions along the chord of a cavitating NACA 0015 hydrofoil in fluoroketone with varying cavitation numbers at fixed angle of attack of 7.5 deg, temperature 25°C, and freestream velocity 6 m/s.**

Although the signal power is weak, some definite trends are visible in the PSD plots shown in Figs. 5, 8, and 11. There are some rogue peaks in the signals: at 7.5 m/s, there is a spike in the static pressure signal at 95 Hz for all conditions and 74 Hz peaks common in the 6 m/s PSD due to the blade passage frequency of the pump impeller. In most cases, the signal power was similar at all points along the hydrofoil, due in part to reduced oscillations of the cavity in supercavitation, similar to tests in water [6]. At $x/c = 0.317$, there is a signal peak at 50 and 100 Hz for every case. The 50 Hz mode equates to $St_c = 0.42$ at $\sigma/2\alpha = 2.67$; the existence of the 100 Hz harmonic is similar to the 5 and 10 Hz signals in a majority of tests in Cervone et al. [6] and Bramanti [7] with $St_c = 0.2$ across most cavitation numbers tested. Gustavsson et al. [8] observed a similar signal with $St_c = 0.56$ at $1.3 < \sigma < 2.6$, and Sato et al. [9] observed $St_c = 0.43$ at $\sigma = 1.25$. At the trailing edge of the hydrofoil, there was an oscillation at 113 Hz in all cases as well. This peak is weaker than the 50 Hz signal but likely represents the separation of the vapor cavity from the hydrofoil. Pressure oscillations seen across several

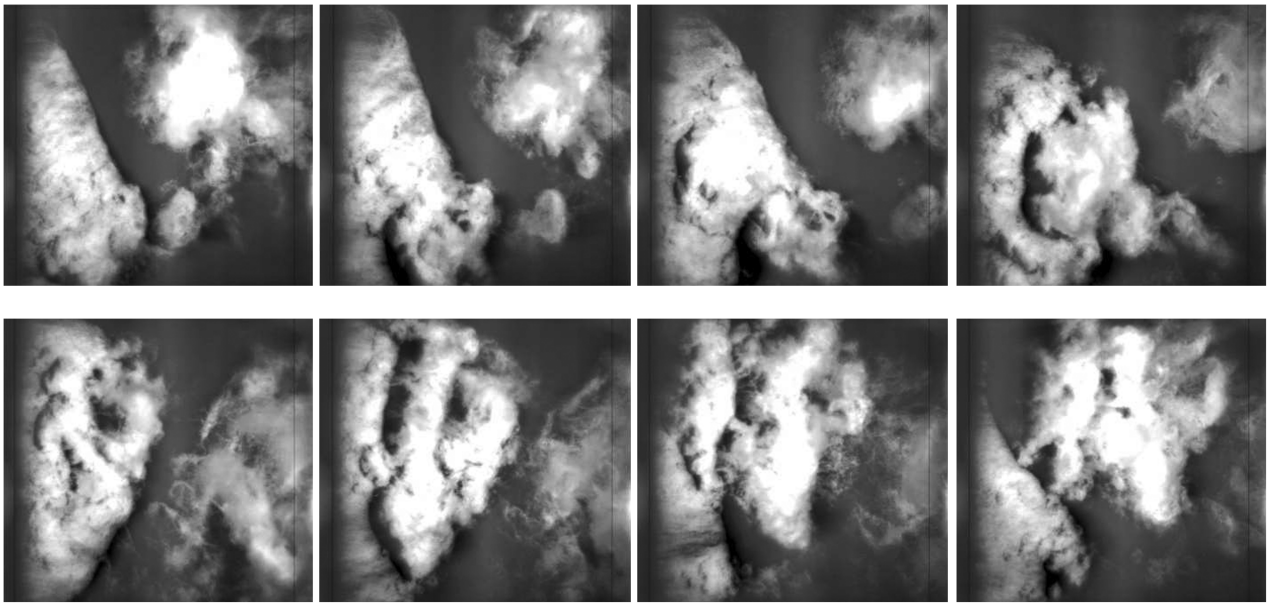

**Fig. 9 Top view of the hydrofoil in case 1 (top) and case 2 (bottom).**



pressure taps are due to fluctuations of the vapor cavity: in other words, the surging and receding of the two-phase region. At the suction peak at $x/c = 0.113$, there is a 123 Hz peak, where $St_c = 0.83$, very similar to the $St_c = 0.82$ peak seen on a flat plate, seen by Sato et al. [9] at $\sigma = 1.5$.

### A. Effect of Velocity

When comparing the effects of velocity, the $Cp$ curves were similar between the two cases (6 and 7.5 m/s), in that the majority of the hydrofoil experienced similar pressure inside of the region where the vapor cavity was present. This pressure was nominally 12% higher than the vapor pressure, showing that dynamic pressure (a function of tunnel speed) has little effect on the pressure inside the vapor cavity and that, even at moderate speeds, supercavitation can become fully developed. The pressure at the leading and trailing edges is close enough to the pressure in a single-phase flow over the hydrofoil to indicate that cavitation is not constant here. Pressure recovery in this region after the peak at $x/c = 0.113$, as can be seen in Fig. 4, was slight but corresponds to the behavior exhibited in supercavitating flows in high-temperature water by Bramanti [7] and in nitrogen by Tani and Nagashima [10]. The onset of cavitation in these regions where the average pressure does not reach the vapor pressure may be due to pressure fluctuations below the vapor pressure that can cause bubbles to propagate downstream [1,4]. The downstream shift of peak ($-Cp$) compared with numerical solutions on a NACA 0015 hydrofoil has been attributed to compressibility effects [11] that are expected in two-phase cryogenic flows. Tests in water [6] do not show this shift.

The $x/c = 0.212$ location saw the biggest deviation in spectral power between test cases. The change in freestream velocity shows that, at this position in Fig. 5, the 6 m/s case, and in Fig. 8, the $\sigma = 1.5$ case show similar broad peaks at 50 and 100 Hz as $x/c = 0.317$ for all cases. This apparent shortening of the average cavity length with raised cavitation number was also seen by Gustavsson et al. [8] in fluoroketone and by Cervone et al. [6] in water up to 70°C at lower angles of incidence but not at higher angles of attack. This supports the conclusions in previous work on fluoroketone that cavitation in thermosensitive fluids at higher incidence angles behaves more like water at lower angles of attack.

The two series of images show a vapor cavity that is wider along the span for the higher speed case. The clouds that are shed from the attached cavity are smaller, and the spatial amplitude of the oscillations along the chord length is reduced. The 6 m/s case shows recession of the cavity to a point where cavitation disappears from the leading edge on one section of the span of the foil, indicative of pressure oscillations strong enough to suppress cavitation even along the leading edge, the laminar-flow pressure drop being the highest at roughly 2% of chord length.

### B. Effect of Cavitation Number

The effect of the cavitation number was isolated by adjusting the pressure in the tunnel while keeping the flow speed and temperature constant. The flat $Cp$ curve in the front portion of the hydrofoil in the $\sigma = 0.7$ case and the strong-peak behavior of the $\sigma = 1.5$ case are seen in Fig. 7. The front of the hydrofoil in the latter, unlike the case with lower $\sigma$, is experiencing higher average pressures due to fluctuations of the vapor cavity over this portion of the chord length. In addition to higher pressure, the ports show a large difference in pressure between the highest and lowest values, close in behavior to noncavitating flow. The strong shift of the case with higher cavitation number toward behavior more like that of cloud cavitation, or more oscillatory motion of the vapor cavity leading to higher average pressures, indicates that the transition from cloud to supercavitation occurs in the pressure range $0.7 < \sigma < 1.5$ akin to tests in water done by Cervone et al. [6].

Despite strong trends in the $Cp$ curve, the effect of the cavitation number showed little dependence in the spectral analysis. There is slightly more power at $x/c = 0.113$ coming from the static signal at $\sigma = 1.5$, and at $x/c = 0.212$, this case shows an almost flat spectral

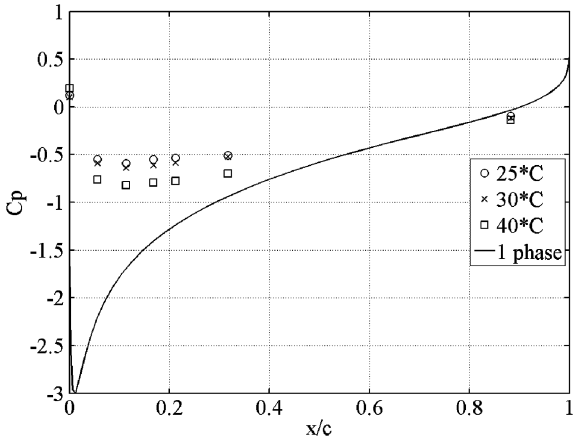


**Fig. 10 Pressure coefficient over a cavitating NACA 0015 hydrofoil in fluoroketone with varying temperature at fixed angle of attack of 7.5 deg, velocity 7.5 m/s, and cavitation number $\sigma = 0.7$.**

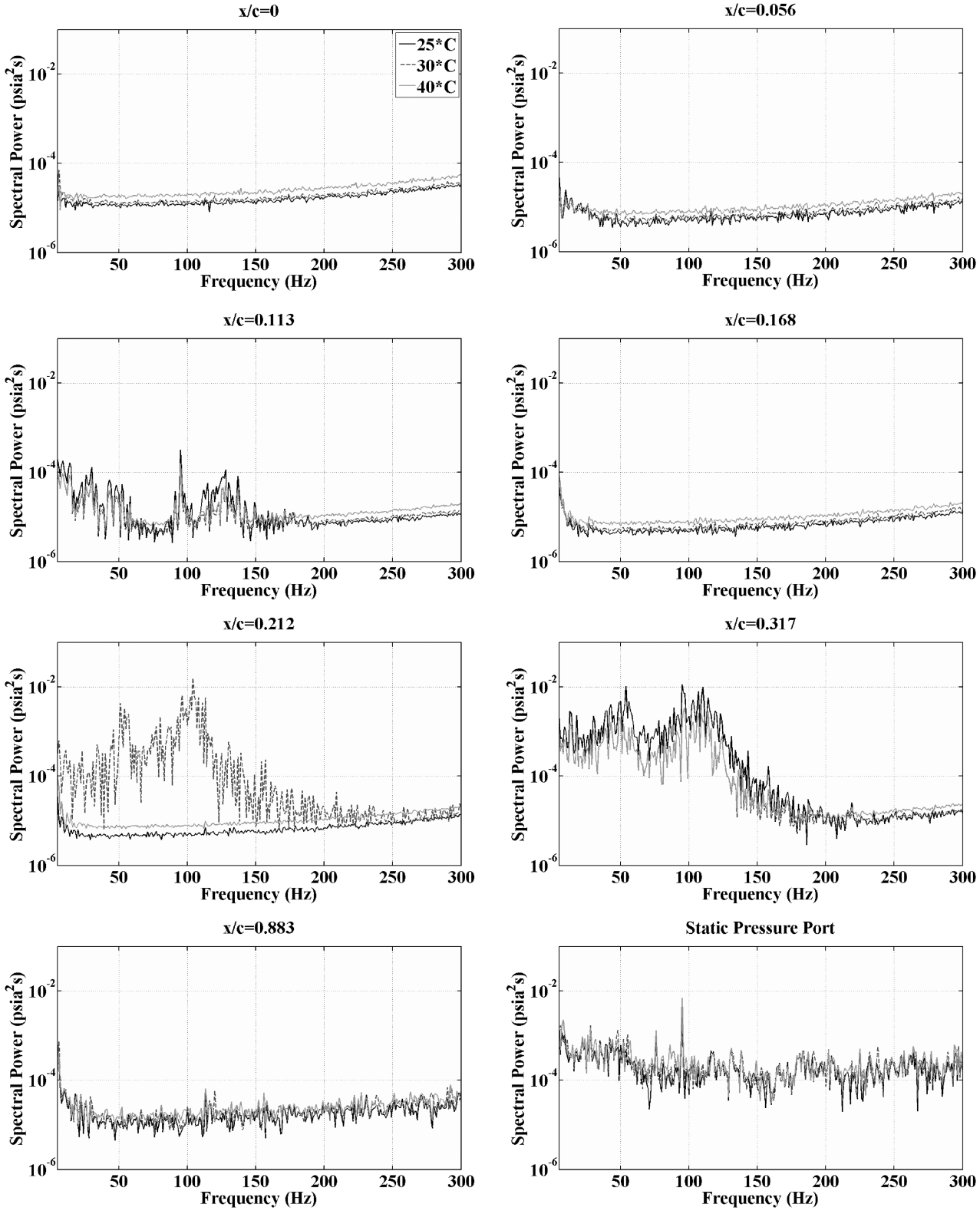


**Fig. 11 Power spectra of static pressure and at various positions along the chord of a cavitating NACA 0015 hydrofoil in fluoroketone with varying temperatures at fixed angle of attack of 7.5 deg, velocity 7.5 m/s, and cavitation number $\sigma = 0.7$.**

response, which may indicate a zone with little action outside the reaches of the oscillating bubble cavity. Hence, changing the cavitation number does not directly cause any strong effects, as are noticed when varying temperature or velocity. Although $\sigma = 1.5$ is very low for most fluids, it may be too similar to $\sigma = 0.7$, and hence does not show any strong trends between the two cases. The images in Fig. 9 show both cavities receding to the leading edge, indicating that the spatial amplitude of the oscillation of the vapor cloud are a function of flow speed. A higher cavitation number shows vapor clouds shed from the attached cavity that are longer with span but shorter along the chord length, with a more consistent shape after detachment. The $\sigma = 0.7$ shed cloud shrinks in cross section faster, indicating more pressure recovery with distance down the hydrofoil, evident in the $Cp$ plot in Fig. 7. Another notable effect is the rougher trailing edge of the cavity with reduced cavitation number, an effect that can also be seen with variation of the velocity, meaning the

congruence of the vapor cavity boundary cannot be attributed to one of these effects alone.

### C. Effect of Temperature

The isolation of temperature in Fig. 10 shows $Cp$ curves with parallel shapes, shifted toward lower $Cp$ with increasing temperature. At higher temperatures, this trend indicates $(-Cp)$ values greater than that of the cavitation number, indicating pressures below the freestream vapor pressure. This is reported in other experiments to be caused by a temperature depression due to absorption of latent heat in the vapor cavity, leading to pressures below the vapor pressure [6,10], and it is supported by numerical analysis as well [12]. Furthermore, the pressure recovery moves even further downstream; this could be due to elongation of the vapor cavity as in [6] or in what is described in [10] as reduced passage, and hence higher pressures due to cavity separation that causes blockage in the flow. This slight change in shape between the case at different temperatures exhibits how the vapor cavity is affected by increasing $\Delta T^*$.

Raising the temperature with the angle of attack kept constant shows a shortening of the cavity; Fig. 11 shows the 30°C case at $x/c = 0.212$ with the same 50 and 100 Hz presence that was manifested in the comparison of velocity. However, the 40°C case showed similar spectra as 25°C. Separation may reduce the effectiveness of signals collected by pressure taps; hence, these effects would be better observed using image analysis, as was done in previous work [4].

With increased temperature comes increased pressure when keeping the flow speed and cavitation number constant, and Fig. 12 shows that the 42% increase in pressure between the 25 and 40°C cases affects cavity length; with the increased pressure comes a shorter attached cavity. In comparison with 30°C, 10% higher pressure than the 25°C case, the cavity lengths are more alike. Higher temperature alone contributes the effect of finer bubble structure, indicative of the effects of thermosensitivity on bubble size and temperature depression in the vapor cavity. Also notable is the more rapid traversal downstream of the detached cloud with increasing temperature. This is an effective increase in the frequency of the shedding of these vapor clouds.

## V. Conclusions

A NACA 0015 hydrofoil was subjected to cavitation at varying cavitation numbers, velocities, and temperatures in a thermosensitive fluid. Pressure measurements were collected along with high-speed imaging. The following conclusions were drawn:

1) Supercavitation develops in thermosensitive fluids, even above the freestream vapor pressure.

2) Fluoroketone experiences a broadening of the pressure peak and slight downstream recovery inside of the vapor cavity similar to that in cryogenic fluids in experimental and numerical tests. Water tends to exhibit a flat $Cp$ curve in this region.

3) A downstream shift of peak $Cp$ is present due to compressibility effects seen in two-phase mixtures present in cryogenics.

4) The stronger peak present in the $Cp$ curve at $\sigma = 1.5$ indicates the transition from cloud to supercavitation exists for $0.7 < \sigma < 1.5$.

5) Tests at higher temperatures showed $(-Cp)$ below freestream vapor pressure due to latent heat absorption at higher values of $\Delta T^*$. Pressure recovery moves farther downstream with increasing $\Delta T^*$ as well.

6) The presence of broad frequency peaks with a strong second harmonic across multiple cavitation numbers was observed, similar to tests in water.

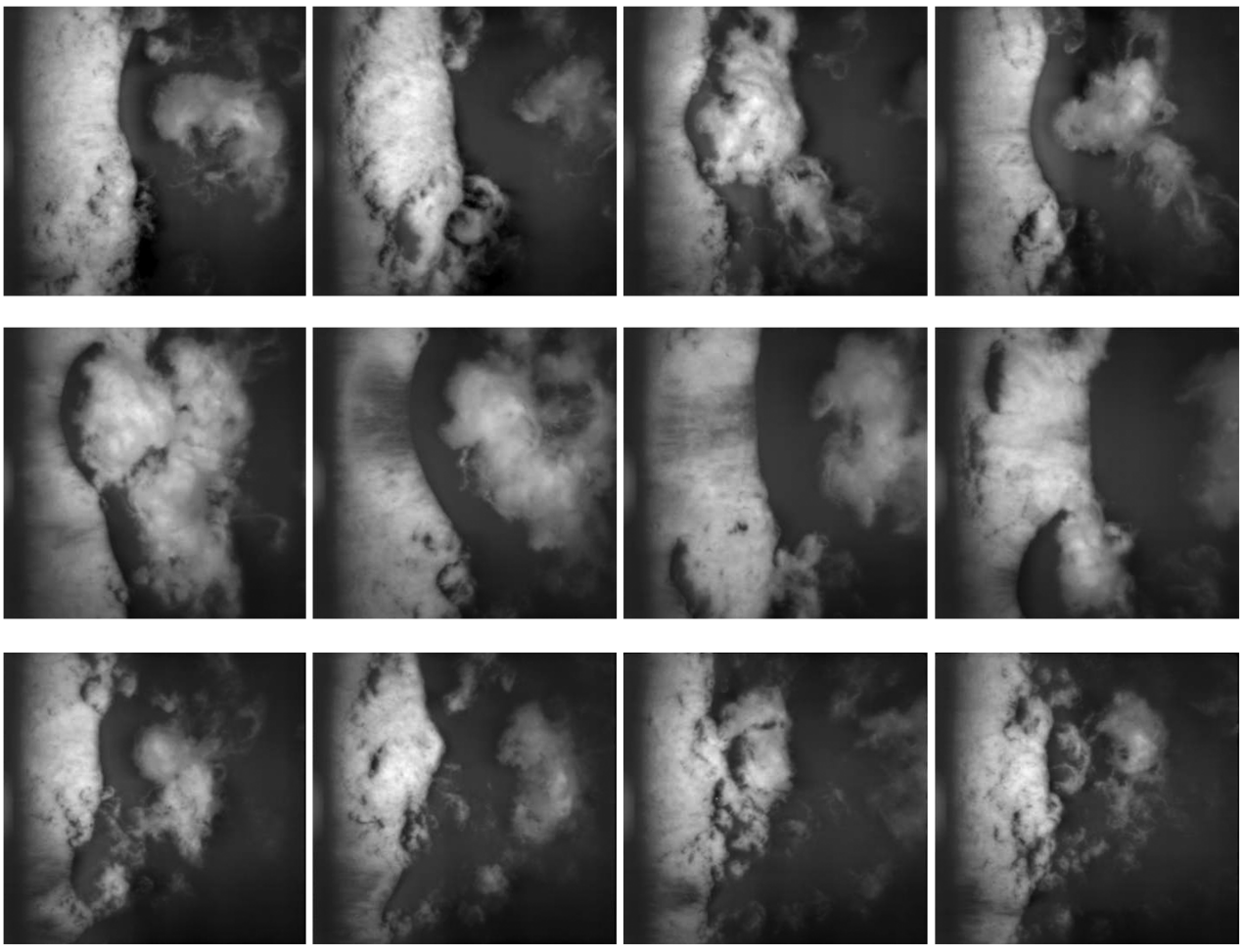

**Fig. 12 Top view of the hydrofoil in case 3 (top), case 4, (middle), and case 5 (bottom).**

7) The vapor cavity shortens with increasing cavitation number. These results support the notion that thermosensitive fluids at higher angles of attack behave like water at lower angles of attack.

## Acknowledgments

This work has been supported by a NASA grant under the Constellation University Institute Program (CUIP). The authors would like to acknowledge the support from Claudia Meyer, the CUIP Manager.

## References

[1] Franc, J.-P., Rebattet, C., and Coulon, A., "An Experimental Investigation of Thermal Effects in a Cavitating Inducer," 5th International Symposium on Cavitation (Cav2003), Osaka, Japan, Paper Cav03-GS-16-001, 2003.

[2] Ruggeri, R. S., and Gelder, T. F., "Cavitation and Effective Liquid Tension of Nitrogen in a Tunnel Venturi," NASA TN D-2088, 1964.

[3] Utturkar, Y., "Computational Modeling of Thermodynamic Effect in Cryogenic Cavitation," Ph.D. Dissertation, Mechanical and Aerospace Engineering Department, Univ. of Florida, Gainesville, Fl, 2005.

[4] Gustavsson, J., Segal, C., and Dorney, D., "Incipient Cavitation Studied Under Strong Thermodynamic Effect," *AIAA Journal*, Vol. 47, No. 3, 2009, pp. 710–716. doi:10.2514/1.38987

[5] Brennen, C. E., *Cavitation and Bubble Dynamics*, Oxford Univ. Press, New York, 1994.

[6] Cervone, A., Bramanti, C., Rapposelli, E., and d'Augostino, L., "Thermal Cavitation Experiments on a NACA 0015 Hydrofoil," *Transactions of the ASME*, Vol. 128, No. 2, 2006, pp. 326–331. doi:10.1115/1.2159025

[7] Bramanti, C., "Experimental Study of Cavitation and Flow Instabilities in Space Rockets, Turbopumps and Hydrofoils," Ph.D. Dissertation, Univ. of Pisa, Pisa, Italy, 2006.

[8] Gustavsson, J., Segal, C., and Dorney, D., "Hydrofoil Cavitation Under Strong Thermodynamic Effect," *Journal of Fluids Engineering*, Vol. 130, No. 9, 2008, Paper 091303. doi:10.1115/1.2953297

[9] Sato, K., Tanada, M., Monden, S., and Ysujimoto, Y., "Observations of Oscillating Cavitation on a Flat Plate Hydrofoil," Fourth International Symposium on Cavitation (CAV2001), Pasadena, CA, Paper Cav-0516, 2001.

[10] Tani, N., and Nagashima, T., "Cryogenic Cavitating Flow in 2D Laval Nozzle," *Journal of Thermal Science*, Vol. 12, No. 2, 2003, pp. 157–161. doi:10.1007/s11630-003-0058-0

[11] Seifert, A., and Pack, L. G., "Oscillatory Control of Shock-Induced Separation," *Journal of Aircraft*, Vol. 38, No. 3, 2001, pp. 486–495. doi:10.2514/2.2788

[12] Tani, N., and Nagashima, T., "Numerical Analysis Of Cryogenic Cavitating Flow On Hydrofoils—Comparison Between Water and Cryogenic Fluids," *Proceedings of 4th International Conference on Launcher Technology*, Liege, Belgium, 2002.

R. Lucht
*Associate Editor*